Nano Energy (2014) 3, 1–9

Available online at www.sciencedirect.com

ScienceDirect

journal homepage: www.elsevier.com/locate/nanoenergy

RAPID COMMUNICATION

Kinetically enhanced pseudocapacitance of conducting polymer doped with reduced graphene oxide through a miscible electron transfer interface

Han-Saem Park, Myeong-Hee Lee, Ryeo Yun Hwang, Ok-Kyung Park, Kiyoung Jo, Taemin Lee, Byeong-Su Kim*, Hyun-Kon Song**

Ulsan National Institute of Science and Technology (UNIST), Interdisciplinary School of Green Energy, 100 Banyeon-ri, Eonyang-eup, Ulsan 689-798, Republic of Korea

Received 1 August 2013; accepted 6 October 2013
Available online 12 October 2013

KEYWORDS
Pseudocapacitance;
Supercapacitors;
Graphene;
Conducting polymers;
Electron transfer

Abstract
Herein, we report on electrochemical doping of a conducting polymer (CP) with anionically modified graphene nanosheets. The architecture built from reduced graphene oxide (rGO) skeleton skinned by polypyrrole (pPy) enhanced supercapacitor performances especially at high discharge rates superior to those of the same CP with a conventional dopant: e.g., from 141 to 280 F g^{-1} at 1000C equivalent to ~50 A g^{-1}. At relatively low rates, the graphene-doped pPy reached the theoretical capacitance of pPy, indicating efficient use of whole electroactive mass.

Introduction

Graphene has attracted a plethora of attention from a variety of areas of science and technology with its remarkable intrinsic properties including electronic [1-4], thermal [5] and mechanical characteristics [6,7]. However, there would be a limitation in direct incarnation of its bulk properties unless a continuous monolithic phase were used [4,8-11]. Particulated forms of graphene or its equivalents have been widely used with the intention to use its superior electronic conductivity in energy applications [12-16]. Even if performances of energy devices

Abbreviations: CP, conducting polymer; rGO, reduced graphene oxide; pPy, polypyrrole; EDLCs, electric double layer capacitors; LIBs, lithium ion batteries; pSS, polystyrenesulfonate; GO, graphene oxide

*Corresponding author. Tel.: +82 52 217 2923; fax: +82 52 217 2019.
**Corresponding author. Tel.: +82 52 217 2512; fax: +82 52 217 2909.
E-mail addresses: bskim19@unist.ac.kr (B.-S. Kim), philiphobi@hotmail.com, philiphobi@gmail.com (H.-K. Song).

2211-2855/$ - see front matter © 2013 Elsevier Ltd. All rights reserved.
http://dx.doi.org/10.1016/j.nanoen.2013.10.001

have been successfully improved by the help of graphene, the fast electron movement would be limited in an isolated dimension of graphene. To fully materialize the properties of graphene in electrochemical devices, electron transfer steps (i) between graphene nanosheets as well as (ii) between the graphene phase and electroactive materials should not be a rate determining step. The main point of this work focuses on how to control or improve the second impeding step of electron transfer.

Electrochemical capacitors have been considered as an energy storage device to deliver electricity especially for high power demand applications [17]. Despite their low energy density, the electrochemical capacitors offer a complementary performance to rechargeable batteries due to their outstanding performances at high discharge rates. The distinguished difference in application sector between the two devices is based on its working principle: non-faradaic processes for electrochemical capacitors (e.g. electric double layer capacitors or EDLCs) and faradaic reactions for rechargeable batteries (e.g. lithium ion batteries or LIBs). Pseudocapacitors (capacitors based on pseudocapacitance) are situated between EDLCs and LIBs, delivering higher energy density than that of EDLCs and working more feasibly at higher power density than LIBs doing. CPs have been one of the favorite choices for pseudocapacitors, based on reduction and oxidation (redox) of charge complex sites or polarons on their backbones. While capacitance of CPs (practically, 200–300 F g^{-1}) is lower than that of metal oxides (400–500 F g^{-1}) that is another option for pseudocapacitance [18], it is still superior to that of EDLCs ($\sim$100 F g^{-1}) [19].

Various efforts have been devoted to building composites consisting of conducting polymers and graphene or its family (graphene oxide (GO) and rGO) to enhance capacitance (Table S1). The composites were made by mixing together graphenes and CPs physically [20] as well as by introducing graphenes into films or powders of CPs during polymerization [21–25]. In most of works of the latter case, small-molecular dopants such as Cl^-, [20,21,23] dodecylbenzene surfonic acid, [22] p-tolenesulfonate, [25] ClO_4^- [21] and NO_3^- [26] were used during polymerization of CPs in presence of GO or rGO. GO has anionic functional groups so that it has a potential to be used as a dopant electrostatically incorporated into CPs [21,24,26]. However, rGO would be physically and statistically entrapped in CPs when monomers are polymerized because rGO contains little amount of anionic functional groups [23,25]. Anionically modified GO obtained by sulfonation were used in presence of an anionic dopant [22]. The sulfonated GO would be more effective as a dopant due to its higher anionic charge concentration. In the work, however, dodecylbenzene sulfonate was used to support doping process during polymerization. As the case in which GO was used as a single dopant in absence of other molecular anions, GO-doped pPy film was electrochemically synthesized [24]. However, electrochemical performances would be kinetically limited due to poor conductivity of GO.

In this work, therefore, we used rGO that is more conductive version of GO for making rGO-doped pPy. Problems of rGO are its poor solubility in water and little anionic characteristics so that rGO was anionically modified with polystyrenesulfonate (pSS) before being used in polymerization. The bridged contact between pPy and rGO through pSS in pPy doped with rGO-pSS (pPy[rGO-pSS]) provided facilitated charge transfer, delivering kinetically robust capacitance.

Materials and methods

Synthesis of graphene oxide (GO)

Graphene oxide (GO) is synthesized from graphite powder (Aldrich, $<$20 μm) by modified Hummers method [27]. In a pretreatment step that ensures complete oxidation, graphite powders (1 g), $K_2S_2O_8$ (0.5 g) and P_2O_5 (0.5 g) were added to 3 mL of conc. H_2SO_4 with stirring until the reactants are completely dissolved. The mixture is kept at 80 °C for 4.5 h using a hotplate, after which the heating is stopped and the mixture diluted with 1.0 L of deionized water. The mixture is filtered and washed to remove all traces of acid. The solid is transferred to a drying dish and left overnight under ambient conditions. For the oxidation step of the synthesis, the pretreated graphite is added to the 26 mL of H_2SO_4 and stirred. To this suspension, 3 g of $KMnO_4$ was added slowly in an ice bath to ensure the temperature remained below 10 °C. Then, this mixture reacts at 35 °C for 2 h after which distilled water (46 mL) is added. Since the addition of the water causes the temperature of the mixture to rise rapidly, it is carried out in an ice-bath so that the temperature does not climb above 10 °C. This mixture is stirred for 2 h at 35 °C, after which the heating is stopped and the mixture diluted with 140 mL of water and 2.5 mL of 30% H_2O_2 is added to the mixture resulting in a brilliant yellow color along with bubbling. The mixture is then allowed to settle for at least a day after which the clear supernatant is decanted. The remaining mixture is filtered and washed with a 1.0 L of 10% HCl solution. The resulting solid is dried in air and diluted in distilled water that is put through dialysis for 2 weeks to remove any remaining metal. The residual products was centrifuged and washed several times with distilled water to neutralization and removal of residual species. Finally, the dark brown GO powders were obtained through drying at 50 °C in vacuum oven for a day. The GO powder was dissolved in a known volume of water (conc. 0.50 mg mL^{-1}) and subjected to ultrasonication for 40 min to give a stable suspension and centrifuged at 4000 rpm for 10 min to recovered supernatant (typically top 90%).

Synthesis of pSS-functionalized reduced graphene oxide (rGO-pSS)

The resulting GO suspension (20.0 mL, 0.50 mg mL^{-1}) was mixed with 0.911 mL of polystyrene sulfonate (pSS, Na salt, Aldrich) solution (1:20 w/w ratio versus GO, 18 wt% dispersion in water). To this solution, 60.0 μL of hydrazine solution (35 wt% in water, Aldrich) was slowly added and the reaction mixture was heated to 100 °C for 1.5 h to afford a stable suspension of reduced graphene oxide (rGO) nanosheets functionalized with pSS (rGO-pSS). After the reaction, the suspension was filtered with poly(ether sulfone) (pES) membrane filter (pore size of 0.22 μm, Corning) and washed extensively with Millipore water to remove any residual

hydrazine and unbound pSS polymer, yielding a thin nanocomposite film of rGO-pSS. After drying under ambient condition, this hybrid thin film is redispersed with a known volume of water at a concentration as high as 0.40 mg mL^{-1}.

Electropolymerization and electrochemical measurements

An electrochemical quartz crystal microbalance (EG&G Seiko/QCA922) connected to a potentiostat/galvanostat (Biologic/VMP3) was used with three-electrode configuration: an AT-cut, 9 MHz gold-plated quartz crystal resonator as the working electrode (area = 0.2 cm^2); a platinum wire as the counter electrode; and Ag/AgCl as the reference electrode. Electrolytes were purged with nitrogen for 5 min just before doing electrochemistry and then curtained with nitrogen during electrochemical experiments. pPy[rGO-pSS], pPy[pSS] was electrodeposited in an aqueous mixture of 200 mM pyrrole and 0.04 wt% rGO-pSS (1.74 mM styrene sulfonate) or 200 mM pSS (the concentration is based on the monomer unit) by cycling potential 80 times or once between −0.7 V and +1.0 V at a scan rate of 50 mV s^{-1}. Pyrrole (Aldrich) in an original bottle was divided into a proper amount in separate glass vials, stored at 4 °C to depress oxidation by atmospheric oxygen and moisture and used as received for electropolymerization. Mass of the polymer films on resonators were measured by an ultramicrobalance (Mettler Toledo, XP6U, readability at 0.1 μg). The mass of pPy[rGO-pSS] calculated from frequency change by Sauerbrey's equation [28] was seriously underestimated and deviated from the mass measured by the ultramicrobalance. However, both measurements provided close values for pPy[pSS]. The electrochemical properties of the electrodeposited films were measured in an aqueous solution of 1 M $LiClO_4$.

Analysis

Scanning and transmission electron microscope (SEM, FEI/NOVASEM 230; TEM, JEOL/JEM-2100, 1400) and atomic force microscope (AFM, Veeco/Multimode V) were used to investigate surface morphology of pPy films. Surface profiler (KLA-Tencor/P-6) as well as AFM were used to estimate thickness of pPy films. Composition of pPy films was determined by elemental analysis including combustion analysis (Thermo Scientific/Flash 2000), inductively coupled plasma atomic emission spectroscopy (ICP-AES, Varian/720-ES) and energy dispersive spectroscopy (EDS, Ametek/Apex-2 SDD).

Results and discussion

Motivation of pPy[rGO-pSS]

The motivation of this work comes from a picture in which electron moves from a current collect to graphene, flows through the graphene as a highway and finally reaches the electroactive sites of CPs through a miscible interface where graphene and CP cannot be distinguished in terms of charge transfer. We achieved the well electron-transferred interface of graphene/CP by doping pPy with functionalized rGO (Figure 1a). rGO is the material succeeding the bulleting electronic conductivity of graphene (electronic conductivity $\kappa_e = 10^{-1}$-10^{0} S cm^{-1} for rGO [29] versus $\sim 10^{6}$ S cm^{-1} for grapheme [30]). By modified Hummer's protocol, [27] graphite was exfoliated into its constituent planes with oxidized functional groups, which is called graphene oxide (GO). GO is easily solubilized in water due to its hydrophilic functional groups with low electronic conductivity caused by breakdown of delocalization of π electrons ($\kappa_e = 10^{-4}$-10^{-3} S cm^{-1} for GO) [29]. The conductivity is recovered not completely but fairly by reducing GO to rGO or removing functional groups. During the reduction step, pSS was introduced to an aqueous suspension of GO in presence of a reducing agent (the first step in Figure 1a). Attributed to the attractive force between aromatic rings of pSS and C_6 units of rGO leading to π-π stacking, pSS was attached to the plane of rGO with a fairly strong force that cannot be easily overcome by a simple excitation such as ultrasonication (rGO-pSS) [31].

pPy, as one of the most representative CPs, is synthesized chemically or electrochemically by oxidizing its monomers. During the polymerization, cationic sites along the polymeric chain are developed every three to ten monomeric unit [32]. Therefore, anionic dopants are required to be incorporated into pPy to neutralize polymeric backbones. pSS is a popular dopant for CPs with a sulfonate group at every repeating unit, guaranteeing conductivity and providing structural security. In this work, a film of pPy[rGO-pSS] was formed on the surface of metal electrodes by applying an anodic potential,. By cycling potential between −0.7 V and +1.0 V versus Ag/AgCl, a stepwise growth of the film was observed as the pyrrole monomers are oxidized at potential higher than 0.5 V, until 40 cycles after which film growth began to saturate (Figure S1). Since there were no significant amount of anions except for rGO-pSS in the monomer solution, the mass and current increases are dominantly related to the formation of pPy[rGO-pSS].

We believe that the dominant phase of resulting CPs synthesized in the presence of two different dopants would not be the graphene-doped phase because graphene is kinetically hard to be incorporated. The growth rate of pPy[rGO-pSS] was estimated much slower than that of pPy[pSS] (pPy doped with pSS; Figure S1) and pPy[pSS]/rGO-pSS (a physical mixture of pPy[pSS] and rGO-pSS; Figure S4) partly for the reason. Another reason explaining the slow growth would be ohmic polarization leading to polymerization overpotential due to low ionic conductivity of electrolyte containing rGO-pSS.

pPy[rGO-pSS] morphology and component ratio

The morphology of rGO was reflected in the pPy[rGO-pSS] film with characteristic wrinkles while pPy[pSS] shows cumulus-like morphology (Figure 1). From its cross-sectional morphology, pPy[rGO-pSS] was much coarser or porous than its pPy[pSS] counterpart, having a free volume significantly caused by the wrinkling constituent, rGO (Figure S2). By using elemental analysis based on combustion method and inductively coupled plasma atomic emission spectroscopy (ICP-AES), the quantitative composition of

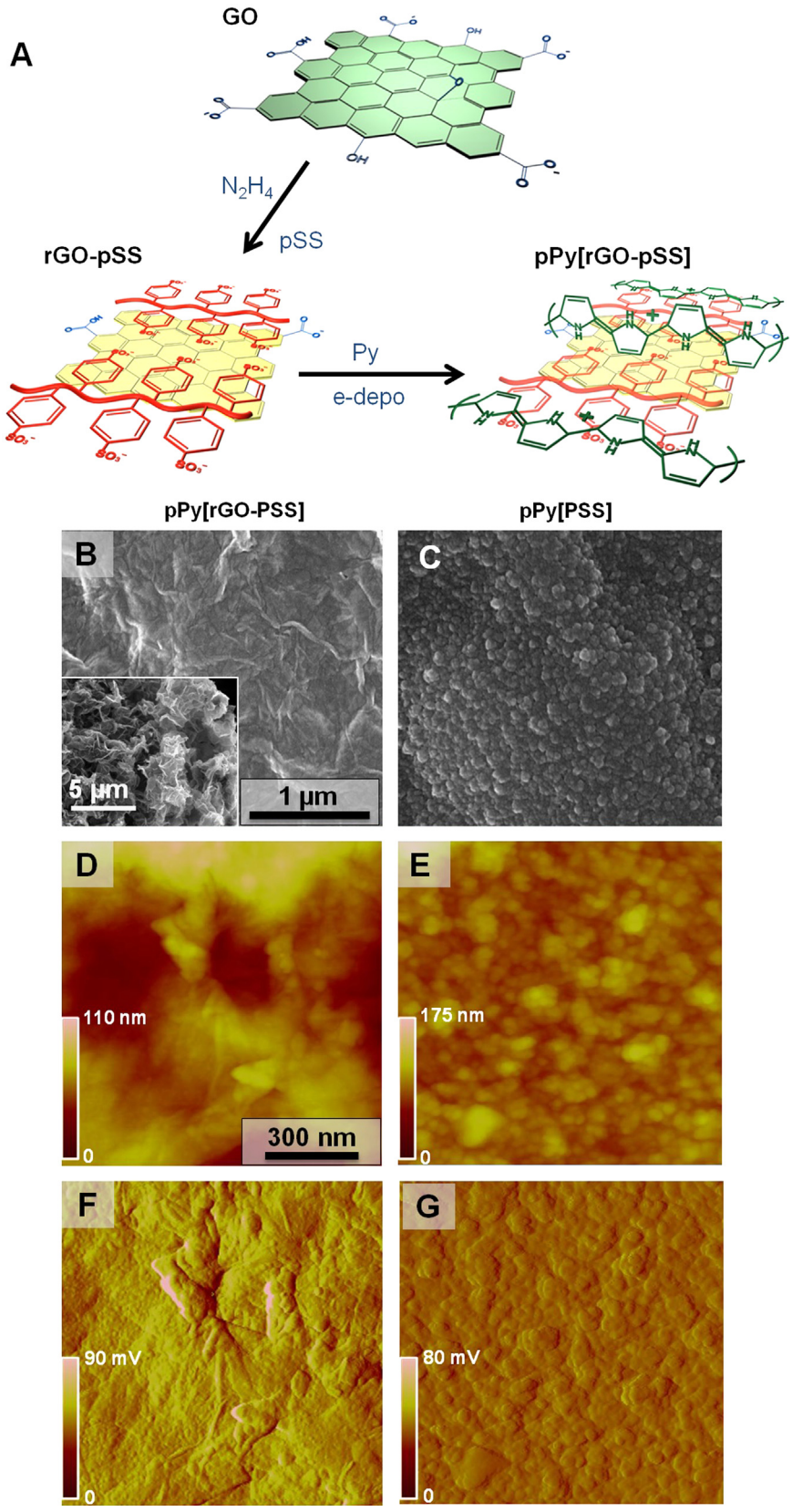

Figure 1 (a) Schematic of pPy[rGO-pSS] obtained by reducing GO in presence of pSS and then electropolymerizing pyrrole in presence of rGO-pSS. (b-g) Morphological images of pPy[rGO-pSS] (left column) and pPy[pSS] (right column) by scanning electron microscope (SEM, b and c) and atomic force microscope (AFM, d and e for height and f and g for amplitude). The scale bar is given for SEM images in (b) and for AFM images in (d). Inset in (b): SEM image of rGO with their own scale bar.

pPy[rGO-pSS] was sketched. One sulfonate group attached to every two C_6 unit of rGO was incorporated into every four monomeric units of pPy: $Py_4 \cdot SS \cdot 2C_6$ where Py=monomeric unit of pPy and SS=styrene sulfonate. The formula of pPy [pSS] was $Py_4 \cdot SS$.

Electrochemical properties of pPy[rGO-pSS] and pPy[pSS]

Capacitance, its rate capability and electrochemical stability as a triumvirate of evaluation criterion of energy devices were clearly improved by graphene doping. The amount of charge stored by pseudo-capacitance based on redox reactions of pPy (C_φ) as well as formation of electric double layer (C_{dl}) was investigated by cyclic voltammograms (Figure 2a and b). The scan-rate dependency of peak current, in which $i_p \propto v^1$ (i_p=peak current and v=scan rate) (insets), indicates that surface-confined redox reactions are responsible for the charging and discharging processes of both pPy[rGO-pSS] and pPy[pSS]. On the other hand, the current or the amount of charge is distinguishably different, with pPy[rGO-pSS] showing very significantly enhanced capacity. Differential capacitance at peak current ($C^D=dq/dV=i_p/v$; q=charge, V=potential) and integral capacitance ($C^I=\int idt/\Delta V=\int(i/v)dV/\Delta V$) were compared between the pPy films (Figure 2c). C^D can be considered as a maximum capacitance while C^I is an averaged value of capacitance over the corresponding potential range. Higher gravimetric capacitances were obtained at 10 mV s^{-1} with pPy[rGO-pSS] (C^D=324 F g^{-1} from peak currents and C^I=243 F g^{-1} for ΔV=0.8 V), which are 28 or 16% enhanced from those of pPy[pSS] and ~2 times as high as those of pPy[pSS]/rGO-pSS (Figure S5). More importantly, the experimental value of C^I for pPy[rGO-pSS] at the slowest scan rate is exactly consistent with the capacitance value calculated from its formula ($Py_4 \cdot SS \cdot 2C_6$) (244 F g^{-1}). In this calculation, capacitance of graphene was assumed to be 170 F g^{-1}(=10 uF $cm^{-2} \times 1700$ m^2 g^{-1} with a half of possible maximum surface area). Therefore, it can be concluded that the theoretical capacitance of pPy contents is fully and efficiently realized in pPy[rGO-pSS]. On the other hand, only 78% of theoretical capacitance (267 F g^{-1} based on $Py_4 \cdot SS$) was reached in pPy[pSS]. In terms of the rate capability, also, pPy[rGO-pSS] showed little decay of capacitance without loss of energy even at kinetically fast scan of potential while its counterpart experienced marked decrease of capacitance: C^D(300 mV s^{-1})/C^D(10 mV s^{-1})=95% for pPy[rGO-pSS] versus 66% for pPy[pSS].

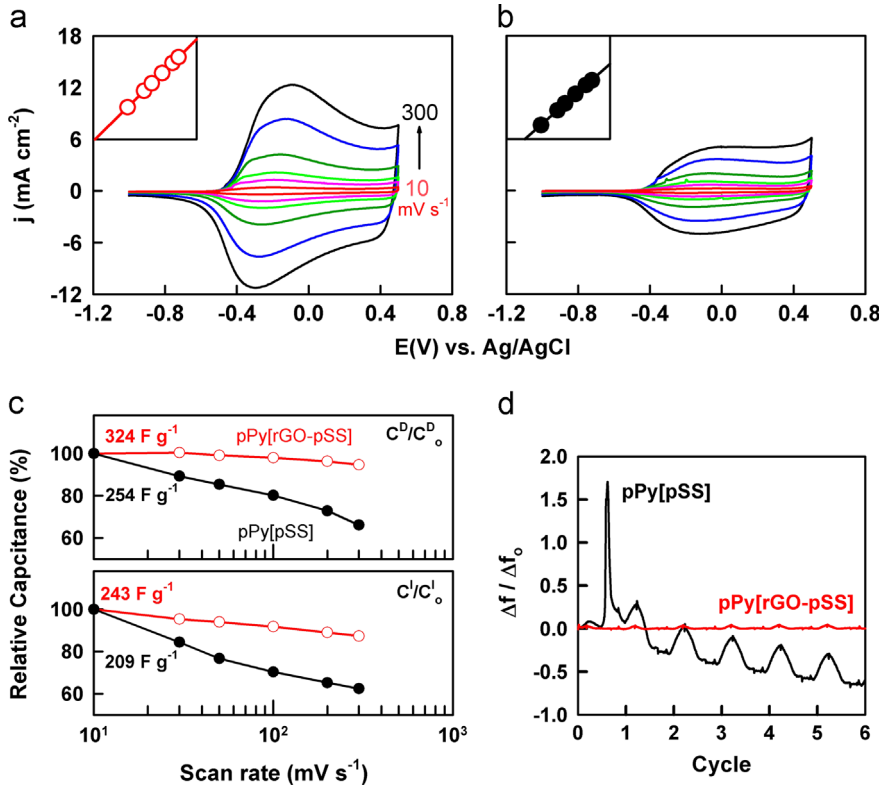

Figure 2 Potentiodynamic electrochemical properties of pPy[rGO-pSS] versus pPy[pSS]. (a and b) Cyclic voltammograms (CVs) and scan-rate dependency of peak current. CVs were obtained at 10, 30, 50, 100, 200 and 300 mV s^{-1} with an aqueous electrolyte of 1 M $LiClO_4$. Apparent area of electrodes (0.2 cm^2) was used to normalize current. Insets: peak current density (mA cm^{-2}) versus scan rate (mV s^{-1}) in an equi-span log-log scale. The slopes were estimated at around 1.0 for both cases. (c) Relative capacitances: C=capacitance; superscript D: calculated by dividing peak current by scan rate; superscript I=calculated from integrating CVs over the voltage range from −0.4 V to +0.4 V; subscript o=the value at the lowest scan rate (10 mV s^{-1}). C^D_o and C^I_o were indicated as the initial values. Mass of films is 25.9 μg for pPy[rGO-pSS] and 20.2 μg for pPy[pSS]. The masses were confirmed by an ultramicrobalance. (d) Temporal change of frequency during potentiodynamic cycling at 100 mV s^{-1}. The frequency change during cycling (Δf) was normalized by the frequency change measured during polymerization (Δf_o).

As the last evaluation criterion, electrochemical stability was investigated by electrochemical quartz crystal microbalance (EQCM) by checking the change of frequency (that can be converted to mass via Sauerbrey's equation if the films were confirmed non-viscoelastic, rigid and thin enough [33]) during cyclic voltammograms. There was no significant change of frequency (Δf) observed with pPy[rGO-pSS] along the progress of cycling, except for the mass change related to an ion exchange behavior within a cycle (Figure 2d). However, pPy[pSS] and pPy[pSS]/rGO-pSS (Figure S5c) experienced a radical change of frequency from the initial cycle in a direction to mass decrease, indicating electrochemical instability which is the ordinarily presupposed demerits of organic materials.

The results from galvanostatic charge/discharge cycling were consistent with those of the potentiodynamic cycling (CVs), confirming that pPy[rGO-pSS] transcends its counterpart (Figure 3). Capacitance of the graphene-incorporated polymer estimated at 301 F g^{-1} at 10 C to 280 F g^{-1} at 1000 C, superior to that of pPy[pSS] with 218 F g^{-1} at 10 C to 141 F g^{-1} at 1000 C (70 F g^{-1} at 1000 C for pPy[pSS]/rGO-pSS in Figure S6). The C-rates ranging from 10 C to 1000 C are very fast charge or discharge rates that are not usually used for testing rechargeable batteries: e.g., 1000 C means the current at which cells can be charged or discharged within 3.6 s (=1 h/1000). From the viewpoint of stability, pPy[rGO-pSS] satisfied an axiom that the efficiency of discharge to charge should be less than 100% due to the unavoidable energy loss caused by internal resistances (Figure 3e). However, pPy[pSS] showed unexpected irreversible faradaic side-reactions during discharge especially at low discharge rate (10 C), which is clearly indicated by 190% efficiency. Therefore, Figure 2d and Figure 3e supports the role of graphene incorporated into CPs to enhance electrochemical stability of pPy[rGO-pSS] in addition to its function as an electronic pathway. The stability of pPy[rGO-pSS] was confirmed up to 100 galvanostatic cycles at 1000 C with only 2.6% reduction of capacitance (Figure S3; less than 0.02% decrease per each cycle up to 100,000 cycles). Graphene would function as a structural prop on which pPy is formed, depressing phase separation between reduced pPy (Py^0_6) and anionic dopant (SS-) in $Py^0_4 \cdot SS^- \cdot C_6$ during reduction; and keeping the reversibility of re-doping of SS- to oxidized pPy (Py^{6+}) during oxidation.

Electron transfer and miscible interface

The miscible interface bridging rGO and pPy through anionic functional groups of rGO-pSS doped into pPy should be emphasized. pPy is conductive in its oxidized state (Py^+_n; > -0.5 V) while it turns insulating in its reduced state (Py^0_n; < -0.5 V). Impedance behaviors can be interpreted in terms of (1) electron conduction within a single phase and (2) electron transfer between two different phases. From the quantitative viewpoint, fast conduction through rGO lead to high double layer capacitance (C_{dl}) by efficiently using electrode–electrolyte interface at the same frequency

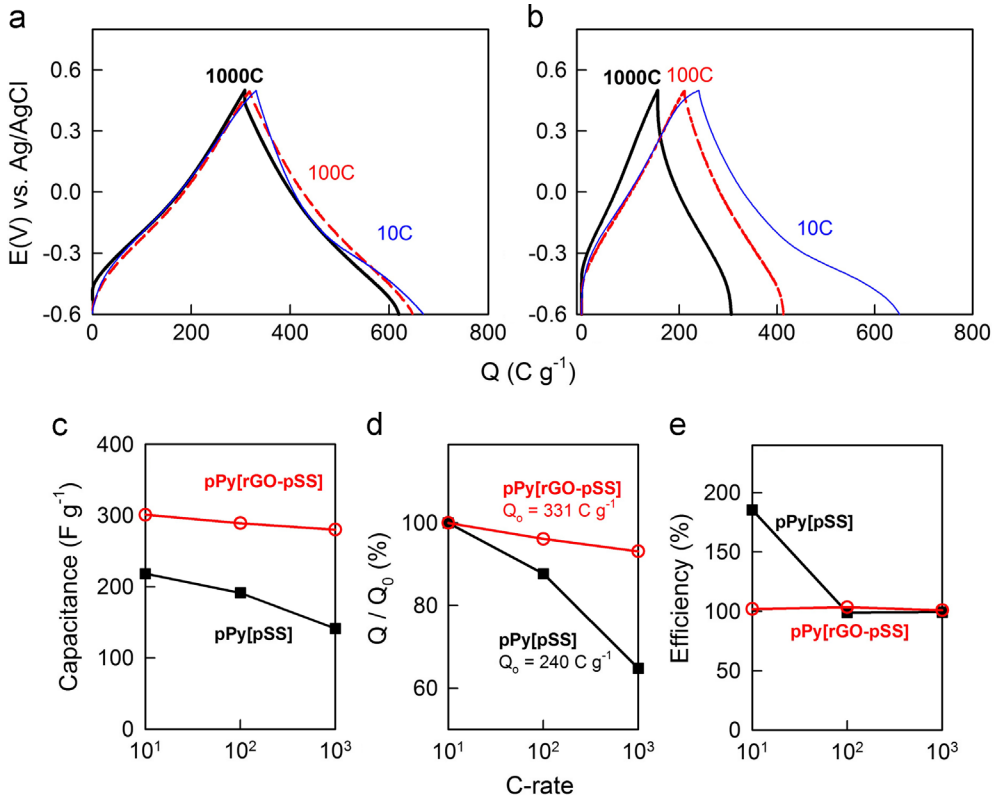

Figure 3 Galvanostatic electrochemical properties of pPy[rGO-pSS] versus pPy[pSS]. (a and b) Charge and discharge profiles. (c–e) Scan rate dependency of capacitance (c), relative capacity (d, Q/Q_o) and efficiency (e). The same electrolyte was used as indicated in Figure 2. 1 C rate was defined as the current at which stored energy was extracted for 1 h. 1.0 C=55 mA g^{-1} for pPy[rGO-pSS] and 45 mA g^{-1} for pPy[pSS].

or stimulus as well as by suppressing development of impedance (pPy[rGO-pSS] over pPy[pSS] at all potentials in Figure 4). On the other hand, both pPy films followed the same qualitative trends of impedance changes depending on biased potentials. In a fully oxidized state at +0.5 V (Figure 4a), electron transfers through Ed|rGO, Ed|Py_n^+ and rGO|Py_n^+ (Ed=current collector) are facile enough to show a purely capacitive behavior (C_{dl}=61 F g^{-1} for pPy[rGO-pSS] and 34 F g^{-1} for pPy[pSS]). Low electron transfer activation energy is expected at the interfaces between two different materials or phases, both of which have fast conduction properties (e.g. metal|metal). In a partially reduced state at −0.5 V (Figure 4b) that is located around the cathodic peaks of CVs, the insulating phase Py_n^0 begins to be developed. The interfaces between Py_n^0 and other phases (Ed, rGO and Py_n^+) limit electron transfer rates, among which Py_n^0|Py_n^+ dominantly affects total electron transfer behavior. There is still a significant difference of capacitance values from low frequency lines (C_{dl}=40 F g^{-1} for pPy[rGO-pSS] and 17 F g^{-1} for pPy[pSS]). In a fully reduced state of pPy[pSS] at −1.0 V (Figure 4c), electron transfer at Ed|Py_n^0 between seriously different phases in terms of their electronic properties was significantly limited with a high value of R_{CT} (=770 Ω mg, τ=310 ms). On the other hand, the miscible interface at rGO|Py_n^0 in pPy[rGO-pSS], bridging electronically different phases via molecular doping, showed a distinguishably improved electron transfer property indicated by a small value of R_{CT} (=182 Ω mg, τ=70 ms). The miscible interface bridging rGO and pSS in pPy[rGO-pSS] is clearly different from the interface between rGO and pPy in pPy[pSS]/rGO-pSS. The physical mixture showed much higher charge transfer resistances and much lower capacitances compared with pPy[rGO-pSS], which is caused by sluggish electron transfer between rGO and pPy of pPy[pSS]/rGO-pSS (Figure S7).

We developed the miscible interface bridging rGO and pPy through anionic functional groups of rGO-pSS doped into pPy by using in situ electropolymerization. pPy[rGO-pSS] exhibited

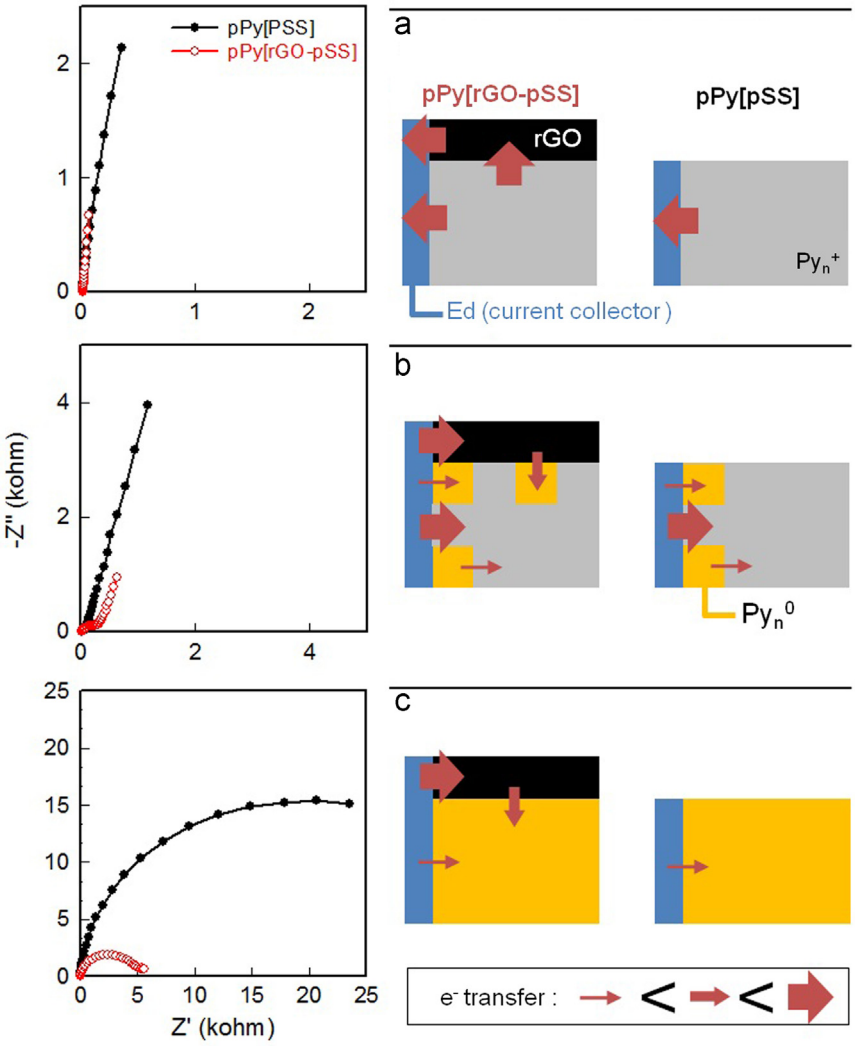

Figure 4 Nyquist plots of impedance measured at three different representative potentials: (a) +0.5 V at which polypyrrole (pPy) is fully oxidized, (b) −0.5 V at which pPy is partially reduced and (c) −1.0 V at which pPy is fully reduced. Schematic illustrations with the corresponding Nyquist plots explain electron transfer kinetics at various solid-to-solid interfaces. The thickness of arrows is proportional to how facile electron transfer is. Thick, middle and thin arrows lead to purely capacitive behavior, small and large charge transfer resistances, respectively.

higher capacitance especially at high discharge rates at $\sim 50\ A\ g^{-1}$ (1000 C) as well as better cycle life, superior to pPy[pSS]. The miscible interface enabled only 7% decrease of capacitance at 1000 C relative to that of 10 C with theoretical capacitance of pPy reached at low discharge rates. Less than 0.02% of capacitance decreased every cycle up to 100,000 cycles.

The facile charge transfer through the miscible interface would originate from three aspects. (1) pPy was tethered by sulfonate groups of pSS to the surface of rGO. Physical contact between pPy and rGO is improved in a way close to each other. In other words, chemical compatibility is mediated by the functional doping. (2) pPy is homogenously composited with rGO in a molecular level (two Py with three C_6 of rGO) by doping. Phase separation caused by single constituent agglomerates (pPy or rGO) can be avoided, which is possibly observed in a physical mixture of the pair. (3) rGO-pSS (or GO) has its own zeta potential around −50 mV. The surface charge can impede electron transfer in a physical mixture of pPy and rGO-pSS. In pPy[rGO-pSS], however, the negative charge of rGO-pSS is neutralized by the positive charge of pPy developed during synthesis.

Conclusion

We believe that it should be the main direction of R&D efforts in application areas of graphene to engineer the interface between graphene and a combined other material. From the electrochemical point of view, an interfacial resistance related to charge transfer rather than bulk resistance is more important for enhancing electrochemical reactions on the electrodes. We regard this work as one of the examples in which the improvement of interfacial miscibility in terms of electronic properties enables a particulate form of graphene to maximize expressing its own intrinsic property. By the help of electronic highway of graphene with the miscible interface with pPy, ultrahigh enhancement of capacitance of pPy was achieved.

Acknowledgments

This work was supported by MOTIE (Green: 10042948(KEIT), Inter-ER:R0000491) and MSIP (CRC: 2013K000210), Korea.

Appendix A. Supplementary material

Supplementary data associated with this article can be found in the online version at http://dx.doi.org/10.1016/j.nanoen.2013.10.001.

References

[1] K.S. Novoselov, A.K. Geim, S.V. Morozov, D. Jiang, Y. Zhang, S.V. Dubonos, I.V. Grigorieva, A.A. Firsov, Science 306 (2004) 666.
[2] A.K. Geim, K.S. Novoselov, Nat. Mater. 6 (2007) 183.
[3] J.S. Wu, W. Pisula, K. Mullen, Chem. Rev. 107 (2007) 718.
[4] K.S. Kim, Y. Zhao, H. Jang, S.Y. Lee, J.M. Kim, J.H. Ahn, P. Kim, J.Y. Choi, B.H. Hong, Nature 457 (2009) 706.
[5] A.A. Balandin, S. Ghosh, W.Z. Bao, I. Calizo, D. Teweldebrhan, F. Miao, C.N. Lau, Nano Lett. 8 (2008) 902.
[6] S. Stankovich, D.A. Dikin, G.H.B. Dommett, K.M. Kohlhaas, E.J. Zimney, E.A. Stach, R.D. Piner, S.T. Nguyen, R.S. Ruoff, Nature 442 (2006) 282.
[7] C. Lee, X.D. Wei, J.W. Kysar, J. Hone, Science 321 (2008) 385.
[8] D. Li, M.B. Muller, S. Gilje, R.B. Kaner, G.G. Wallace, Nat. Nanotechnol. 3 (2008) 101.
[9] S. Park, J.H. An, I.W. Jung, R.D. Piner, S.J. An, X.S. Li, A. Velamakanni, R.S. Ruoff, Nano Lett. 9 (2009) 1593.
[10] C. Berger, Z.M. Song, X.B. Li, X.S. Wu, N. Brown, C. Naud, D. Mayou, T.B. Li, J. Hass, A.N. Marchenkov, E.H. Conrad, P.N. First, W.A. de Heer, Science 312 (2006) 1191.
[11] X.S. Li, W.W. Cai, L. Colombo, R.S. Ruoff, Nano Lett. 9 (2009) 4268.
[12] M.D. Stoller, S.J. Park, Y.W. Zhu, J.H. An, R.S. Ruoff, Nano Lett. 8 (2008) 3498.
[13] S.J. Guo, D. Wen, Y.M. Zhai, S.J. Dong, E.K. Wang, ACS Nano 4 (2010) 3959.
[14] H.L. Wang, L.F. Cui, Y.A. Yang, H.S. Casalongue, J.T. Robinson, Y.Y. Liang, Y. Cui, H.J. Dai, J. Am. Chem. Soc. 132 (2010) 13978.
[15] Y.Q. Sun, Q.O. Wu, G.Q. Shi, Energy Environ. Sci. 4 (2011) 1113.
[16] Y.W. Zhu, S. Murali, M.D. Stoller, K.J. Ganesh, W.W. Cai, P.J. Ferreira, A. Pirkle, R.M. Wallace, K.A. Cychosz, M. Thommes, D. Su, E.A. Stach, R.S. Ruoff, Science 332 (2011) 1537.
[17] J.R. Miller, P. Simon, Science 321 (2008) 651.
[18] Y. Zhang, H. Feng, X.B. Wu, L.Z. Wang, A.Q. Zhang, T.C. Xia, H.C. Dong, X.F. Li, L.S. Zhang, Int. J. Hydrogen Energy 34 (2009) 4889.
[19] L.L. Zhang, X.S. Zhao, Chem. Soc. Rev. 38 (2009) 2520.
[20] J.H. Liu, J.W. An, Y.X. Ma, M.L. Li, R.B. Ma, J. Electrochem. Soc. 159 (2012) A828.
[21] H. Wang, Q. Hao, X. Yang, L. Lu, X. Wang, Electrochem. Commun. 11 (2009) 1158.
[22] A. Liu, C. Li, H. Bai, G. Shi, J. Phys. Chem. C 114 (2010) 22783.
[23] D.C. Zhang, X. Zhang, Y. Chen, P. Yu, C.H. Wang, Y.W. Ma, J. Power Sources 196 (2011) 5990.
[24] H.H. Chang, C.K. Chang, Y.C. Tsai, C.S. Liao, Carbon 50 (2012) 2331.
[25] J.P. Wang, Y.L. Xu, J.B. Zhu, P.G. Ren, J. Power Sources 208 (2012) 138.
[26] L.W. Hu, J.G. Tu, S.Q. Jiao, J.G. Hou, H.M. Zhu, D.J. Fray, Phys. Chem. Chem. Phys. 14 (2012) 15652.
[27] W.S. Hummers, R.E. Offeman, J. Am. Chem. Soc. 80 (1958) 1339.
[28] G. Sauerbrey, Z. Phys. 155 (1959) 206.
[29] V. López, R.S. Sundaram, C. Gómez-Navarro, D. Olea, M. Burghard, J. Gómez-Herrero, F. Zamora, K. Kern, Adv. Mater. 21 (2009) 4683.
[30] J.H. Chen, C. Jang, S.D. Xiao, M. Ishigami, M.S. Fuhrer, Nat. Nanotechnol. 3 (2008) 206.
[31] S. Stankovich, R.D. Piner, X.Q. Chen, N.Q. Wu, S.T. Nguyen, R.S. Ruoff, J. Mater. Chem. 16 (2006) 155.
[32] H.-K. Song, E.J. Lee, S.M. Oh, Chem. Mater. 17 (2005) 2232.
[33] R.Y. Hwang, S.Y. Kim, G.T.R. Palmore, H.-K. Song, J. Electroanal. Chem. 657 (2011) 181.

Han-Saem Park received his B.S. degree in mechanical engineering at the Kyungpook University in 2010, and he is now a graduate student in the Interdisciplinary School of Green Energy at UNIST. He is currently working on supercapacitors using conducting polymers.

Myeong-Hee Lee received her B.S. and M.S. in Polymer Science & Engineering at the Pusan National University of Korea in 2001 and 2003 respectively. She is a researcher of Interdisciplinary School of Green Energy at UNIST and currently working on graphene-doped conducting polymers for pseudocapacitance via a miscible interface.

Ryeo Yun Hwang received her M.S degree in a chemistry department from the Pusan National University in 2008, and she is now a Ph.D. candidate in the Graduate School of Analytical Science & Technology at Chungnam National University. She is currently working on DMFC(direct methanol fuel cell) using Solid-State NMR.

Ok-Kyung Park received her B.S. and M.S degrees in department of chemistry at Pukyung National University. Currently, she is a Ph.D. candidate of UNIST.

Kiyoung Jo received his B.S. in electrical engineering and material science engineering at UNIST in 2013. Currently he is a graduate student in school of natural science at UNIST. The research field is hybrid structure of 2-dimensional nanosheets for device application.

Taemin Lee received his B.S. in nano-engineering at the Inje University of Korea in 2010, and he is now a graduate student in the Interdisciplinary School of Green Energy at UNIST. He is currently working on the synthesis and assembly of graphene oxide-based hybrid nanomaterials.

Byeong-Su Kim is an Assistant Professor of Interdisciplinary School of Green Energy at Ulsan National Institute of Science and Technology (UNIST) since 2009. He received his B.S and M.S. degrees in chemistry from Seoul National University. In 2007, he received his Ph.D in polymer/nanomaterial chemistry from University of Minnesota. From 2007 to 2009, he worked as a post-doctoral associate at the Massachusetts Institute of Technology (MIT). His current research interests include the chemistry of carbon nanomaterials and their energy and biomedical applications.

Hyun-Kon Song is an associate professor of Interdisciplinary School of Green Energy at UNIST, Korea. He received his Ph.D. in Chemical Engineering from POSTECH, Korea. His career covers postdoctoral researcher at Brown University and Seoul National University; and senior researcher at LG Chem/Research Park. His research disciplines are based on electrochemistry and materials chemistry, covering synthesis of electroactive materials and novel design of electrochemistry-based devices.